Economic Geology, v. 102, pp. 1047–1061

Venting of Acid-Sulfate Fluids in a High-Sulfidation Setting at NW Rota-1 Submarine Volcano on the Mariana Arc

J. A. Resing,† G. Lebon,

Joint Institute for the Study of the Atmosphere and Ocean, University of Washington, and Pacific Marine Environmental Laboratory, National Oceanic and Atmospheric Administration, 7600 Sand Point Way NE, Bldg. 3, Seattle, Washington 98115-6349

E. T. Baker,

Pacific Marine Environmental Laboratory, National Oceanic and Atmospheric Administration, 7600 Sand Point Way NE, Bldg. 3, Seattle, Washington 98115-6349

J. E. Lupton, R. W. Embley,

Pacific Marine Environmental Laboratory, National Oceanic and Atmospheric Administration, 2115 S.E. OSU Drive, Newport, Oregon 97365-5258

G. J. Massoth,

Institute of Geological and Nuclear Sciences, P.O. Box 31-312, Lower Hutt, New Zealand

W. W. Chadwick, Jr.,

Oregon State University and National Oceanic and Atmospheric Administration, Newport, Oregon 97365-5258

and C.E.J. de Ronde

Institute of Geological and Nuclear Sciences, P.O. Box 31-312, Lower Hutt, New Zealand

Abstract

A comprehensive survey of hydrothermal plumes and their geochemistry revealed 16 hydrothermally active volcanoes along 1,200 km of the Mariana arc from 13.5° N to 22.5° N. Of these 16, one volcano, NW Rota-1, is discharging sulfuric acid-rich fluids producing some of the largest chemical anomalies ever observed in nonbuoyant hydrothermal plumes. Two types of venting were observed, one of focused flow rich in Al, S, Si, CO_2, Fe, Mn, and ^3He, and a second of diffuse flow rich in Fe, Mn, CO_2, and ^3He but without Al, S, and Si. The plume waters from the acid-rich focused flow showed decreases in pH up to 0.73 pH units compared to ambient seawater and an estimated 80 percent of this change was brought about by volcanic and/or hydrothermal SO_2 (and possibly HCl) with the remaining 20 percent by CO_2. Conservative estimates suggest that the pH of the venting fluids was <1.0. The chemistry of this plume was also greatly different from that observed in any other hydrothermal setting. An acid-sulfate or high-sulfidation fluid source was indicated from plume water samples rich in sulfuric acid, native S, Al-sulfate-phosphate minerals, and weathered silicate and amorphous silica phases. The alunite group minerals and acidic fluids indicate that the most important hydrothermal reactions taking place within the hydrothermal system were resulting in advanced argillic alteration of the host volcanic rocks. Gas chemistry of the fluids revealed an He isotope signature with $R/R_a = 8.35$ and $^3He/CO_2 = 3.25 \times 10^9$. These values are similar to those found along the global midocean ridge (MOR), suggesting that the source of the ^3He and CO_2 found here is predominantly from the upper mantle, consistent with the position of NW Rota-1 closest to the back arc in a chain of cross-arc volcanoes. The chemical signatures of the plumes arising from the diffuse flow remain greatly enriched in Fe, Mn, ^3He, and CO_2, but compared to the focused flow are low in mineral acidity (H^+), Al, and S. The source of this diffuse flow is likely a fluid similar to that producing the acid-rich plume but with a lower water-to-rock ratio and a longer reaction time, resulting in the consumption of the mineral acidity. This results in an increase in pH and the deposition of the alunite-phosphate-sulfate and other minerals close to the seafloor. By comparison, it is likely that the low-pH focused flow ejects the vast majority of its mineral load into the water column which is not conducive to the formation of a mineral deposit at the sea floor, and potentially would produce a "barren prospect."

Introduction

The direct degassing of magmatic volatiles rich in both SO_2 and CO_2 from submarine volcanic and/or hydrothermal systems has not been directly observed. However, the effects of these volatiles have been documented by the presence of excess sulfate and Mg in hydrothermal fluids (McMurtry et al., 1993; Gamo et al., 1997). The presence of sulfuric acid-rich fluids has also been inferred from the presence of plumes greatly enriched in Al in the Manus basin (Gamo et al., 1993), from plumes with low pH combined with surface-ocean sulfur

† Corresponding author: e-mail, joseph.resing@noaa.gov

slicks above an actively erupting Macdonald seamount (Cheminée et al., 1991), and from plumes over Brothers volcano of the Kermadec arc (de Ronde et al., 2005). It has been suggested that these magmatic volatiles combine with hydrothermal fluids to create an acid-rich magmatic-hydrothermal fluid that is able to greatly alter the host volcanic rocks and may ultimately be responsible for the formation of high-sulfidation–type mineral deposits (Hedenquist, 1995). However, the exact role of magmatic-hydrothermal ore formation has been debated (e.g., Gemmell et al., 2004; Deyell et al., 2005). One suggestion is that chemically specialized magmatic fluids, expelled from crystallizing magma, are already preenriched in ore metals that subsequently react with interstitial water to produce ore deposits. Another hypothesis is that a combination of hydrothermal and magmatic fluids creates an extremely acidic fluid that is able to leach metals from the surrounding volcanic rock.

Hydrothermal ore deposits of volcanic origin are commonly divided into high- and low-sulfidation types (Cooke and Simmons, 2000; Hedenquist et al., 2000). Low-sulfidation hydrothermal systems are characterized by having near-neutral pH, reduced sulfur, and a low water-to-rock ratio. By contrast, high-sulfidation systems are characterized by low pH, oxidized sulfur, and high water-to-rock ratios (Cooke and Simmons, 2000). High-sulfidation hydrothermal deposits are often Au, Cu, and Ag rich and are associated with a complex alteration assemblage including quartz, alunite, clays (pyrophylite, kaolinite, dickite), diaspore, native S, aluminum phosphate sulfate (APS) minerals, and pyrite (Sillitoe et al., 1996; Dill, 2001; Cooke and Simmons, 2000; Hedenquist et al., 2000). These alteration products and associated textures are thought to result from hot acidic fluids reacting with the host rocks, leaving remnant alteration products.

Advanced argillic alteration assemblages typical of high-sulfidation environments have been observed in the submarine settings of the Manus basin (e.g., Gemmell et al., 1999; ODP Leg 193), the Valu Fa ridge of the Lau basin (Herzig et al., 1998), and along the Kermadec arc (de Ronde et al., 2005). These observations as well as those of sulfate-enriched hydrothermal fluids indicate submarine hydrothermal systems with magmatic-hydrothermal fluids and gasses rich in SO_2. Establishing the involvement of magmatic volatiles in the formation of these deposits is thus critical to understanding the possible sources of metals and sulfur in submarine ore-forming environments.

During February-March 2003, a comprehensive survey of hydrothermal plumes and their geochemistry was completed above 50 submarine volcanoes located along the Mariana arc from 13.5° N to 22.5° N (Embley et al., 2004). Sixteen of the submarine volcanoes surveyed were hydrothermally active, with eight showing very intense activity. One volcano, NW Rota-1 (Fig. 1), had hydrothermal plumes containing sulfuric acid, Al-phosphate-sulfate minerals, and native S, indicative of the presence of magmatic volatiles. This volcano was revisited in 2004, 2005, and 2006, using a remotely operated vehicle (ROV) and found to be in a continuous state of eruption (Embley et al., 2006; Chadwick et al., in prep.). This report is the first confirmed finding of alunite group minerals actively venting from a submarine volcano. Although such observations are rare, only relatively few studies have been conducted so far on submarine magmatic arcs and, until recently those

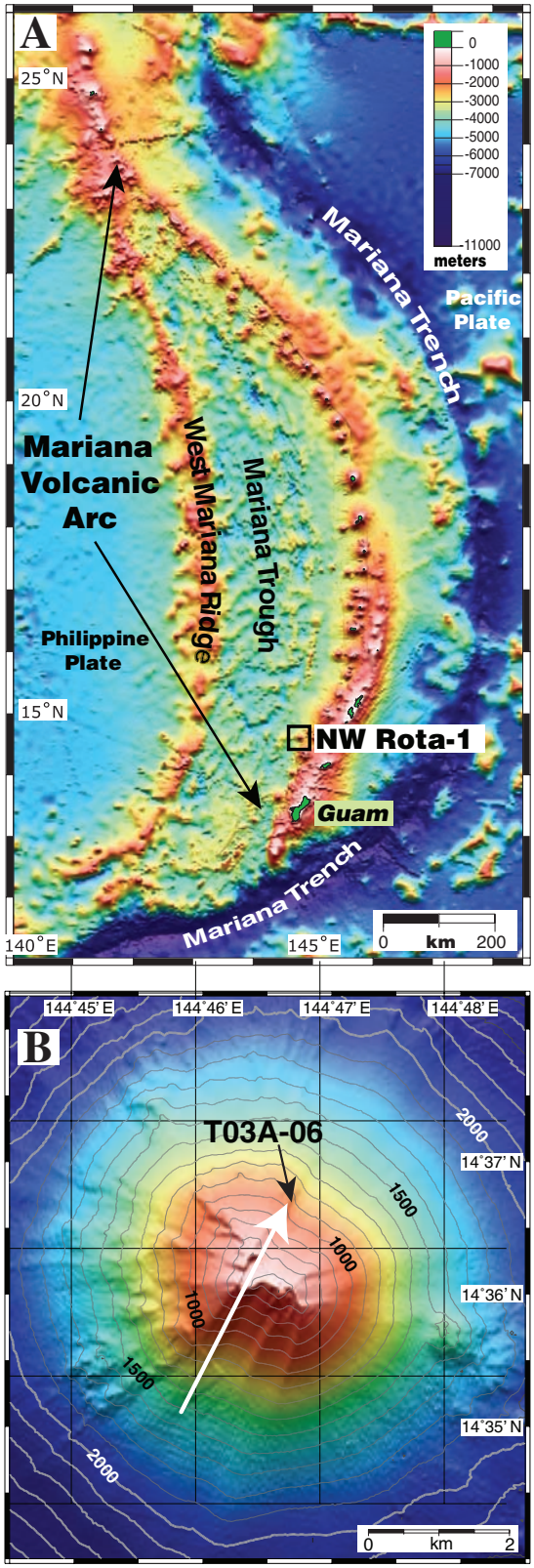

FIG. 1. A. Bathymetric map of the Mariana arc. NW Rota is located north-northwest of the Island of Guam. B. Bathymetric map of NW Rota-1 volcano. The white arrow represents the length and direction of the towed hydrocast over the volcano. Note that the hydrocast is to the western side of the summit and not directly over it. Figure modified from Embley et al. (2006).

studies have not employed the entire suite of measurements needed to fully characterize the nature of these systems.

Regional Setting

The Mariana arc is part of the Izu-Bonin-Mariana arc system, an intraoceanic convergent margin that extends southward more than 2,500 km from Japan to south of Guam (Fig. 1A). Here, the Pacific plate subducts beneath the Philippine plate and is the oldest subducting oceanic lithosphere on Earth. This results in a uniquely cold subduction zone with extraordinarily deep penetration of the subducting slab into the mantle (van der Hilst et al., 1991). These factors suggest that the transport of elements from the slab into the overlying mantle is more likely to be dominated by fluids as opposed to melts when compared to other subduction zones (Peacock, 1990). The volcanic activity along the arc results from the increased fertility of mantle materials due to the release of water from the subducting slab. Peate and Pearce (1998) estimated that ~10 percent of the melting may be attributed to decompression and ~15 to 20 percent to fluid addition.

NW Rota-1 is a submarine volcano located at the western end of a cross-chain of submarine volcanoes that extend west of the magmatic arc front of the Mariana arc, at 14° 36' N, 144° 46.5' E (Fig. 1B). It is conical in shape and about 16 km in diameter at its base at 2,700 m. Its summit lies at 517 m along a ridge between southwest-northeast–trending, inward-facing fault scarps that cut across the volcano. Rock samples collected from NW Rota-1 in 2004 were vesicular, moderately fractionated, medium K basalt and basaltic andesites (51.8% SiO_2, 0.62% K_2O, 6.4% MgO: Stern et al., 2004). One of the adjacent smaller volcanoes, Chaife, located about 25 km east-northeast of NW Rota-1, has unusual high magnesium mafic lavas that Kohut et al. (2006) interpreted as originating from adiabatic melting of an anhydrous portion of mantle wedge.

Methods

The survey of the Mariana arc submarine volcanoes was accomplished using a high-precision Sea Bird 911 plus CTD (conductivity, temperature, depth) package augmented with a light scattering sensor (LSS, Seapoint Inc.). Light scattering anomalies are reported as ΔNTU, which is the difference between the value measured and that of the background. Discrete water samples were collected using a rosette package with 21 18.5-l Niskin-type bottles outfitted with standard sampling spigots for gas collection and Teflon stopcocks for trace metal and trace particulate sample collection.

Samples for total dissolvable Mn and Fe ($Mn_{(total\ dissolvable)}$ and $Fe_{(total\ dissolvable)}$ were collected directly from the Teflon stopcocks into 125-ml I-Chem polyethylene bottles, while dissolved Mn and Fe ($Mn_{(dissolved)}$ and $Fe_{(dissolved)}$) samples were collected as the filtrate from 0.4-μM acid-washed polycarbonate filters into 125-ml I-Chem polyethylene bottles after the passage of 2 l of water through the filters. The samples for metals analysis were then acidified with 0.5 ml of subboiling distilled 6*N* HCl. Mn was determined with a precision of ~1 nM by modifying the direct injection method of Resing and Mottl (1992) by adding 4 g of nitrilo-triacetic acid to each liter of buffer. Fe was determined with a precision of ±2 nM by modifying the method of Measures et al. (1995) for direct injection analysis. Total CO_2 (ΣCO_2) and pH samples were collected and analyzed as discussed in Resing et al. (2004). Changes in pH (ΔpH) and ΣCO_2 (ΔCO_2) were calculated by subtracting the regional background value found at a given depth from the value measured in the plumes at the same depth. Hydrogen sulfide was determined on samples following the procedure of Sakamoto-Arnold et al. (1986). Elemental compositions of particulate matter were determined by X-ray (primary- and secondary-) emission spectrometry with a Pd source and Mo, Ti, Ge, and Co secondary targets using a nondestructive thin-film technique (Feely et al., 1991). Precision averaged 2 percent for major elements, 7 percent for trace elements, and 11 percent for S. The particulate matter contains both the volatile and nonvolatile sulfur; volatile S is defined here as the difference between sequential analyses of S under a nitrogen atmosphere ($S_{(total)}$) and under a vacuum (nonvolatile S). Scanning electron microscope (SEM) images and associated chemical compositions were obtained from an ISI DS130 scanning electron microscope fitted with a Kevex Quantum X-ray detector and IXRF model 500 analyzer and software. Samples for He analysis were drawn immediately after recovery of the CTDO/rosette package and sealed into copper tubing using a hydraulic crimping device (Young and Lupton, 1983). Helium concentrations and helium isotope ratios were determined using a 21-cm radius, dual-collector mass spectrometer. Precision of the ^3He concentration measurements is $\pm 2 \times 10^{-17}$ mol kg^{-1}.

The four parameters, pCO_2, pH, alkalinity, and ΣCO_2, are thermodynamically related and only two of the parameters are required to fully describe the carbonate system (Millero, 1979). These numerical relationships have been incorporated into a computer program (Lewis and Wallace, 1998) that requires the input of salinity, temperature, depth, silica, phosphate, and two of the carbon system parameters to yield the remaining system parameters. Silica and phosphate were estimated from WOCE transect P10 (Sabine et al., 1999).

Results

To determine if hydrothermal activity was present at NW Rota-1, the CTD rosette package and associated sensors were towed (T03A06) to the northwest of the summit of the volcano on February 12, 2003 (Fig. 1). The package was raised and lowered as it passed over the volcano creating the sawtooth pattern shown in Figure 2. The light-scattering sensor (LSS) detected large clouds of particles both above and around the summit of the volcano (Fig. 2), indicating vigorous hydrothermal venting. The most elevated particulate load (largest ΔNTU) was present at ~460-m depth, ~60 m above the summit of the volcano. The tow was conducted to the northwest of the summit, thus the plume is ~200 m above the highest point of the volcano's profile beneath the tow track in Figure 2, which is not the summit of the volcano. The package was stopped at various depths and locations within the hydrothermal plume and 18 samples and two duplicates were collected (locations are identified in Fig. 2). Aliquots were collected for pH, Fe, and Mn from all samples, and a subset of samples was taken for ΣCO_2, particulate matter composition, and dissolved metals. Many of these samples were found to be greatly enriched in a wide range of hydrothermal and magmatic products when compared to background seawater (Fig. 3, Tables 1, 2).

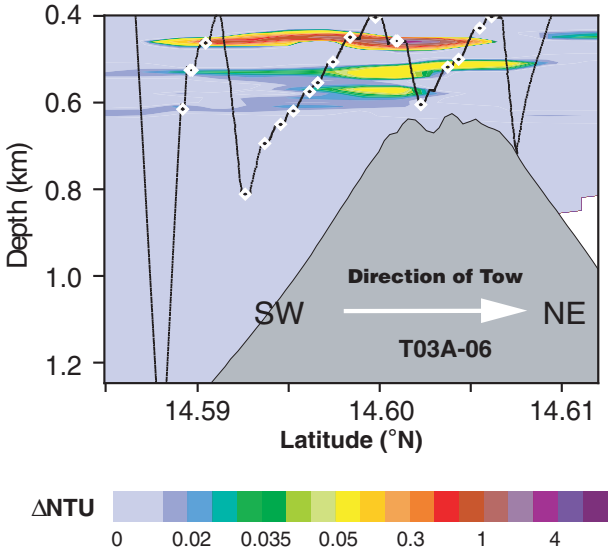

FIG. 2. Cross section of the hydrothermal plumes above the NW Rota-1 volcano, showing elevated optical backscatter above the volcano which delineates the hydrothermal plumes. The black sawtooth pattern is the track of the CTD-Rosette package as it passed over the volcano. The stair step features in the track are the locations where samples were taken and are identified by small white diamonds. The large white arrow indicates the direction of the tow. ΔNTU = nephelometric turbidity units (light scattering due to particles in the water) above ambient seawater.

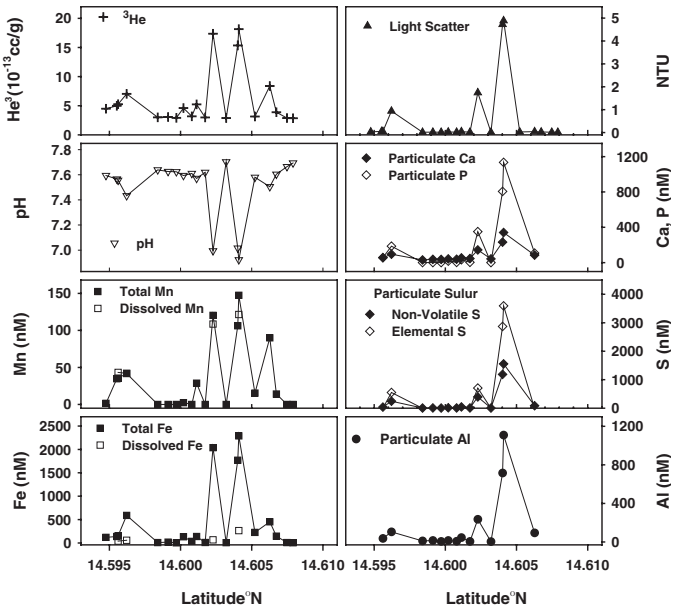

FIG. 3. Chemical composition of samples taken within the hydrothermal plume above NW Rota-1 submarine volcano. Fe, Mn, ^{3}He, and pH were determined on whole water samples. Ca, P, S, and Al were all in the particulate phase. NTU= nepelometric turbidity unit (light scattering due to particles in the water).

Plume distribution

The largest hydrothermal plume was identified at ~460 m, and lesser plumes were found at a variety of depths from ~520 to ~600 m. Hydrothermal venting from the volcano occurs on and near the summit from ~520- to ~590-m depth (Embley et al., 2006). The most intense venting was associated with a small crater (Brimstone Pit) at 550-m depth. Compared to the intense, high discharge venting at the crater, less buoyant flow was found at another hydrothermal site at 530-m depth and likely represents discharge from a number of diffuse sites near the summit resulting from hot fluids rising through unconsolidated volcanic debris. The upper plume at 460-m depth is the most intense plume observed at this site and is almost certainly associated with the most intense venting from the Brimstone pit. The lower plume from 520 to 560 m is less intense and appears to be associated with the more diffuse venting. The plume located at 600 m is much less intense and must result from additional diffuse venting not observed by Embley et al. (2006).

The hydrothermal fluids produced at NW Rota-1 rise in the water column because they are forcefully ejected from the volcano and the warm fluids are more buoyant than the ambient seawater at the depth of the hydrothermal vents. Active high-temperature smokers along midocean ridges produce plumes that typically rise 100 to 250 m above their sources. The midocean ridges are located in the deep ocean where changes in seawater density with depth are minimal and the warm water of lower density rises more easily. Here, in the shallower ocean, the change in density with depth is greater, resulting in a greater resistance to plume rise and thus a lower plume rise height. Despite this stronger gradient in density, the most intense venting observed at NW Rota rises ~100 m, while the less intense venting only rises ~5 to ~10 m. Observations at midocean ridges by Lupton et al. (1985) demonstrate that plumes are likely diluted by a factor of 1,000 to 10,000 or more as they rise from depth. The ~100-m rise of the plume suggests that similar levels of dilution likely take place at NW Rota-1 as well.

Plume chemistry

The plumes over NW Rota-1 were greatly enriched in dissolved and particulate species of metals and gasses. Figure 3 demonstrates the latitudinal distribution of several of the chemical components along the tow over the volcano, with the individual samples identified by white diamonds in Figure 2. The plumes observed at multiple depths have different chemistry (Fig. 4). The upper plume at 460 m showed the highest ΔNTU and the greatest chemical enrichments, while the plumes below 520 m had somewhat smaller enrichments. When the chemical compositions of the plumes are compared (Fig. 5, Tables 2, 3), the difference between the upper and lower plumes is clear.

Particulate matter composition: The ΔNTU observed in the plumes was the result of suspended particulate matter composed primarily of aluminum sulfate, elemental S, and amorphous iron oxyhydroxides. These particles arise from two processes: they vent directly from the volcano, and they precipitate from the hydrothermal fluids as they are diluted and cooled by ambient oxidizing seawater. In the presence of oxygen at lower temperatures, reactions favor the formation of elemental S and, in addition, Al and Fe in the dissolved phase are supersaturated with respect to background seawater.

The chemical composition of the particulate matter in the upper plume is dominated by P, Fe, Si, Al, and S species. The concentrations of these species (Table 1) are extraordinarily

TABLE 1. Dissolved and Particulate Chemistry of Hydrothermal Plumes above NW Rota-1 (all samples from towed hydrocast T03A-06)

		Dissolved chemistry[3]				Particulate chemistry																	
S[1]	TSM[2] (ug/l)	TFe	DFe	TMn	DMn	Na	Mg	Al	Si	P	K	Ca	Ti	V	Cr	Fe	Cu	As	Se	Sr	Ba	W	Pb
		(nmol/l)				(nmol/l)																	
						Upper plume																	
4	-	6	-	0	-	-	-	-	-	-	-	-	-	-	-	-	-	-	-	-	-		-
8	10.1	6	-	0	-	2	3	3	15	1	0.36	42.9	0.09	0.02	0.10	2	0.04	NV	0.00	0.19	0.21	0.00	0.00
34	-	9	-	0	-	-	-	-	-	-	-	-	-	-	-	-	-	-	-	-	-		-
50	490.7	2038	67.6	120.3	109	AN	AN	AN	AN	AN	AN	AN	AN	AN	AN	AN	AN	AN	AN	AN	AN	AN	AN
20	490.5	1770	-	106	-	109	178	715	491	807	18.27	231.9	15.24	3.98	1.96	1513	5.43	4.36	0.23	3.29	4.07	0.15	0.10
10	635.8	2290	264	147	122	318	272	1109	655	1135	26.28	340.9	18.30	5.46	2.60	2053	6.68	5.90	0.25	4.74	NV	0.00	0.13
31	149.5	590	58	42	42	188	53	105	102	187	7.16	96.0	2.97	1.34	0.58	440	0.94	1.21	0.07	1.01	1.51	0.05	0.05
6	-	146		14	-	-	-	-	-	-	-	-	-	-	-	-	-	-	-	-	-		-
						Lower plume																	
30	8.9	10	-	0	-	1	3	5	15	4	0.38	46.3	0.13	0.04	0.04	8	0.03	0.02	0.00	0.21	0.25	NV	0.00
15	78.3	452	-	90	-	18	35	94	78	108	1.77	84.8	1.75	0.99	0.57	298	0.35	0.60	0.02	0.69	1.20	0.03	0.03
3	38.5	155	40	36	43	56	20	36	39	57	1.65	55.9	0.81	0.37	0.23	110	0.56	0.27	0.01	0.38	0.56	.01	0.02
36		137	-	35	-																		
29	33.2	138	-	29	-	16	15	45	66	33	1.93	54.5	1.36	0.26	0.19	84	0.71	0.17	0.00	0.38	0.45	0.01	0.02
24	10.4	35	-	0	-	1	4	7	21	3	0.57	38.5	0.23	0.03	0.05	8	0.03	0.01	0.00	0.18	0.23	0.01	0.01
21	-	226	-	15	-	-	-	-	-	-	-	-	-	-	-	-	-	-	-	-	-		-
26	-	120	-	1	-	-	-	-	-	-	-	-	-	-	-	-	-	-	-	-	-		-
13	18.0	133	-	2	-	8	9	14	37	17	0.97	42.6	0.52	0.12	0.13	42	0.06	0.11	0.00	0.26	0.30	0.02	0.01
17	8.6	4	-	0	-	5	4	5	20	1	0.54	36.7	0.18	0.02	0.09	7	0.09	0.02	0.01	0.18	0.21	0.01	0.00
16	11.5	18	-	0	-	6	6	15	43	1	1.02	37.4	0.49	0.03	0.03	7	0.03	NV	0.00	0.17	0.19	0.01	0.00
2	9.2	9	-	0	-	3	4	10	33	1	0.83	31.3	0.32	0.02	0.02	3.80	0.03	0.01	0.00	0.13	0.17	NV	0.00
						Maximum value of upper plume relative to maximum value of lower plume																	
Ratio		5.1		1.6		5.7	7.7	12	8.4	10	14	6.7[4]	10	5.5	4.6	4.9	6.9	10	17	9.1[4]	3.9[4]	9	5

Notes: AN = analysis not possible, NV = no value, "-" = sample not collected

[1] Sample no.

[2] Total suspended matter

[3] TFe = total dissolvable Fe, DFe = dissolved Fe, TMn = total dissolvable manganese, DMn = dissolved manganese

[4] Background Ca, Sr, and Ba removed

TABLE 2. Dissolved Gases and Acidity in Hydrothermal Plumes above NW Rota-1

Sample no.	Depth (m)	T (°C)	Salinty (PSU)	OBS[1] (NTU)	pH	ΔpH	ΣCO_2 (μM)	ΔCO_2 (μM)	^3He (fM)	Δ^3He (fM)	^4He (fM)	TS[2] (nM)	S NV[3] (nM)	S Vol[4] (nM)	CH_4 (nM)
							Upper plume								
4	403	8.47	34.29	0.014	7.694	0.000			2.9	0.0	1791728				1.6
8	404	8.60	34.29	0.015	7.703	0.000	2216.4	–0.3	2.9	0.0	1798671	2	5	-3	1.7
34	429	8.07	34.32	0.015	7.665	0.000			2.9	0.0	1807099				0.9
50	450	7.81	34.35	1.741	6.994	–0.649	2293.4	47.8	17.4	15.5	3046816	AN	AN	AN	3.1
20	459	7.88	34.34	4.724	7.016	–0.632	2281.3	38.6	15.3	12.4	2890245	4056	1188	2869	2.7
10	459	7.91	34.34	4.891	6.923	–0.726	2292.4	50.0	18.2	15.3	3118897	5150	1556	3594	3.3
31	464	7.89	34.32	0.940	7.433	–0.222	2254.3	14.6	7.0	4.1	2161381	794	244	550	1.7
6	501	7.30	34.40	0.026	7.604	–0.014			3.9	1.0	1901224				1.3
							Lower plume								
30	507	7.32	34.40	0.015	7.619	0.001	2262.0	1.2	3.0	0.1	1812334	2	6	-4	1.4
15	519	7.12	34.41	0.042	7.505	–0.109			8.4	5.5	2291899	71	85	–14	3.5
3	527	7.22	34.41	0.048	7.556	–0.060			5.3	2.3	2022091	35	37	–3	1.9
36	527	7.23	34.41	0.052	7.566	–0.050			5.0	2.1	1992237				1.9
29	555	6.99	34.42	0.039	7.571	–0.041	2284.1	16.2	5.2	2.3	1994207	41	45	–4	2.5
24	576	6.72	34.43	0.017	7.610	–0.002	2272.5	–0.5	3.2	0.2	1836030	4	8	–4	1.2
21	606	6.34	34.44	0.025	7.580	–0.034			3.1	0.2	1889779				4.2
26	617	6.28	34.44	0.029	7.594	–0.021			4.5	1.5	1968900				4.9
13	621	6.21	34.45	0.024	7.594	–0.022	2286.8	5.6	4.6	1.7	1999978	9	14	–5	4.8
17	652	5.96	34.46	0.013	7.624	0.003			2.9	0.0	1824917	1	4	–3	0.6
16	696	5.67	34.47	0.016	7.626	–0.002	2286.9	–1.5	3.1	0.1	1840318	4	6	–3	0.8
2	813	5.11	34.50	0.012	7.639	0.000	2295.0	1.0	3.0	0.0	1849219	2	4	–2	0.4
							Maximum value of upper plume relative to maximum value of lower plume								
Ratio				94		6.7		3.1	2.8	2.8		73	18		0.5

Abbreviations: AN = analysis not possible, fM = femptomolar, nM = nanomolar, PSU = practical salinity units

[1] Optical backscatter (nephelometry turbidity units)

[2] Total sulfur

[3] Nonvolatile sulfur (sulfates + sulfides)

[4] Volatile sulfur (elemental sulfur)

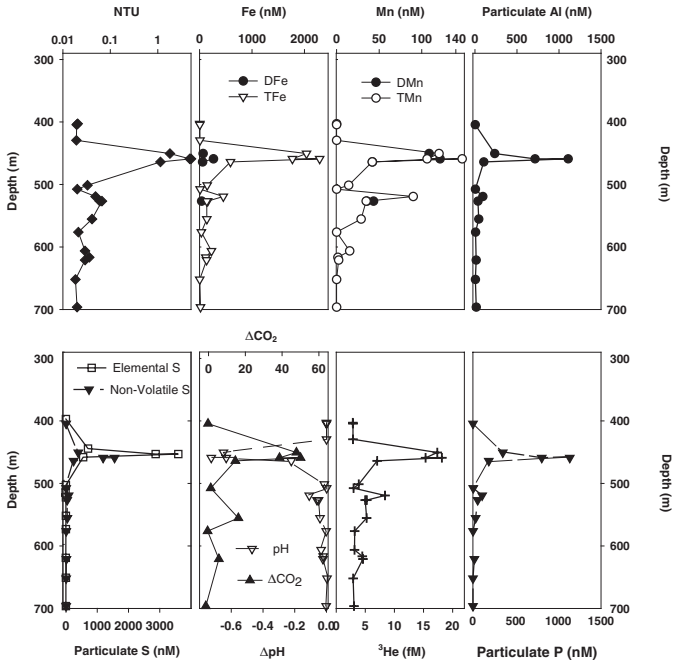

FIG. 4. Composition of the hydrothermal plume as a function of depth above NW Rota-1 submarine volcano. OBS = optical backscatter. Elemental sulfur refers to volatile sulfur.

high compared to background values of ~1 nM for particulate P, Fe, Al, and S, and 25 nM for particulate Si. The particulate P, Fe, Si, Al, and S concentrations are also in excess of those found in typical hydrothermal plumes above midocean ridges, which range from 1 to 50 nM P, 10 to 600 nM Fe, 50 to 200 nM Si, 3 to 20 nM Al, and 1,500 nM S (e.g., Feely et al., 1992).

TABLE 3. Elemental Ratios for Upper and Lower Plumes

	Upper plume Ratio	R^2	Lower plume Ratio	R^2
Particulate matter				
Al/NVS[1]	0.70 ± 0.06	0.99	1.05 ± 0.06	0.98
P/Fe	0.56 ± 0.02	1.00	0.37 ± 0.02	0.98
V/Fe	0.0026 ± 0.001	1.00	0.0033 ± 0.000	1.00
Ratios of $Fe_{(total\ dissolvable)}$ and gases to $Mn_{(total\ dissolvable)}$				
CH_4/Mn	0.013 ± 0.002	0.88	0.014±.018	0.06
ΔCO_2/Mn	0.35 ±. 01	1.00	0.54 ±.09	0.91
^{3}He/Mn	1.09 ± .04 × 10^{-7}	0.99	5.5 ± 0.7 × 10^{-8}	0.85
TFe/Mn	16.0 ± 0.4	1.00	4.2 ±0.7	0.80
Ratios of particulate components to $Mn_{(total\ dissolvable)}$				
Na/Mn	1.6 ± 0.9	0.62	0.28 ± 0.19	0.24
Mg/Mn	1.84 ± 0.15	0.99	0.35 ±.02	0.97
Al/Mn	7.8 ± 1	0.96	0.94 ± 0.06	0.97
Si/Mn	4.61 ± 0.5	0.98	0.57 ±0.14	0.69
P/Mn	8.0 ± 0.7	0.99	1.18 ± 0.07	0.97
S/Mn[2]	37 ± 4	0.98	0.79 ± 0.07	0.95
K/Mn	0.18 ± 0	1.00	0.014 ± 0.005	0.58
Ca/Mn	2.04 ±.18	0.98	0.51 ± 0.05	0.94
Ti/Mn	0.13 ±.02	0.97	0.017 ± 0.003	0.83
Cu/Mn	0.049 ± 0.006	0.97	0.005 ± 0.003	0.37
Se/Mn	0.0019 ± 0.0002	0.97	1.5 ± 0.4 × 10^{-4}	0.70
Sr/Mn	0.032 ± 0.002	0.99	0.0056 ± 0.0004	0.97
Ba/Mn	0.037 ± 0.002	1.00	0.011 ± 0.005	0.98
Pb/Mn	8.9 ± 0.5 × 10^{-4}	0.99	3.0 ± 0.5 × 10^{-4}	0.83

[1] Al to nonvolatile sulfur
[2] Total sulfur to $Mn_{(total\ dissolvable)}$

A single sample in the upper plume was collected for SEM analysis. In addition to visual examination of individual particles, the integrated X-ray fluorescence detector (IXRF) allows the composition of imaged particles to be

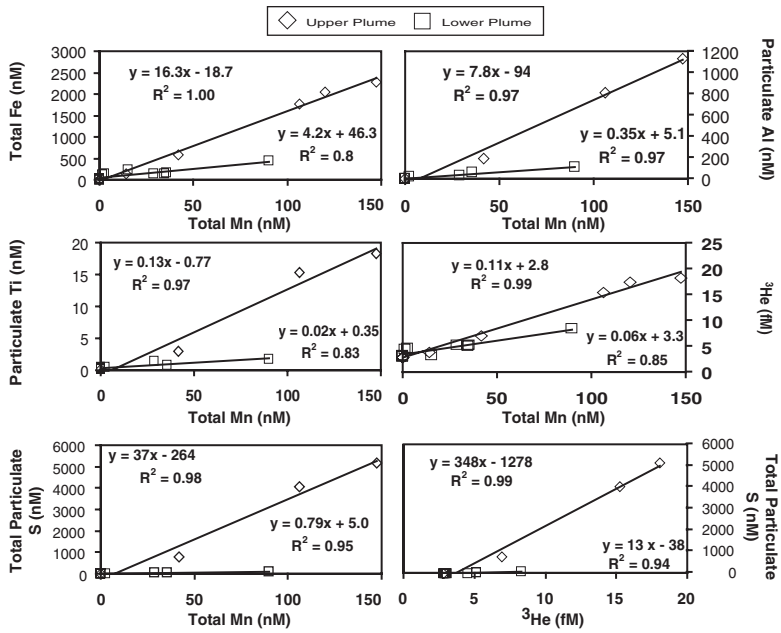

FIG. 5. Comparison of the compositions of the upper and lower plumes at NW Rota-1. The upper plume is enriched in the products of argillic alteration like S, Al, Ti, whereas these components are missing from the lower plume.

determined. The IXRF is capable of both spot analysis and whole-particle mapping; whole-particle mapping is time-consuming, whereas spot analyses are completed in tens of seconds. During the SEM-IXRF analysis, a wide range of particle compositions and morphologies was observed. The most abundant particles found were rich in Si, Fe, S, and Al, whereas less abundant particles contained Ca, Mg, and Na. The Si-rich particles (Fig. 6) were predominantly freshly precipitated amorphous Si and leached rock. The less abundant Si-rich phases included clays (Fig. 7) and, more rarely,

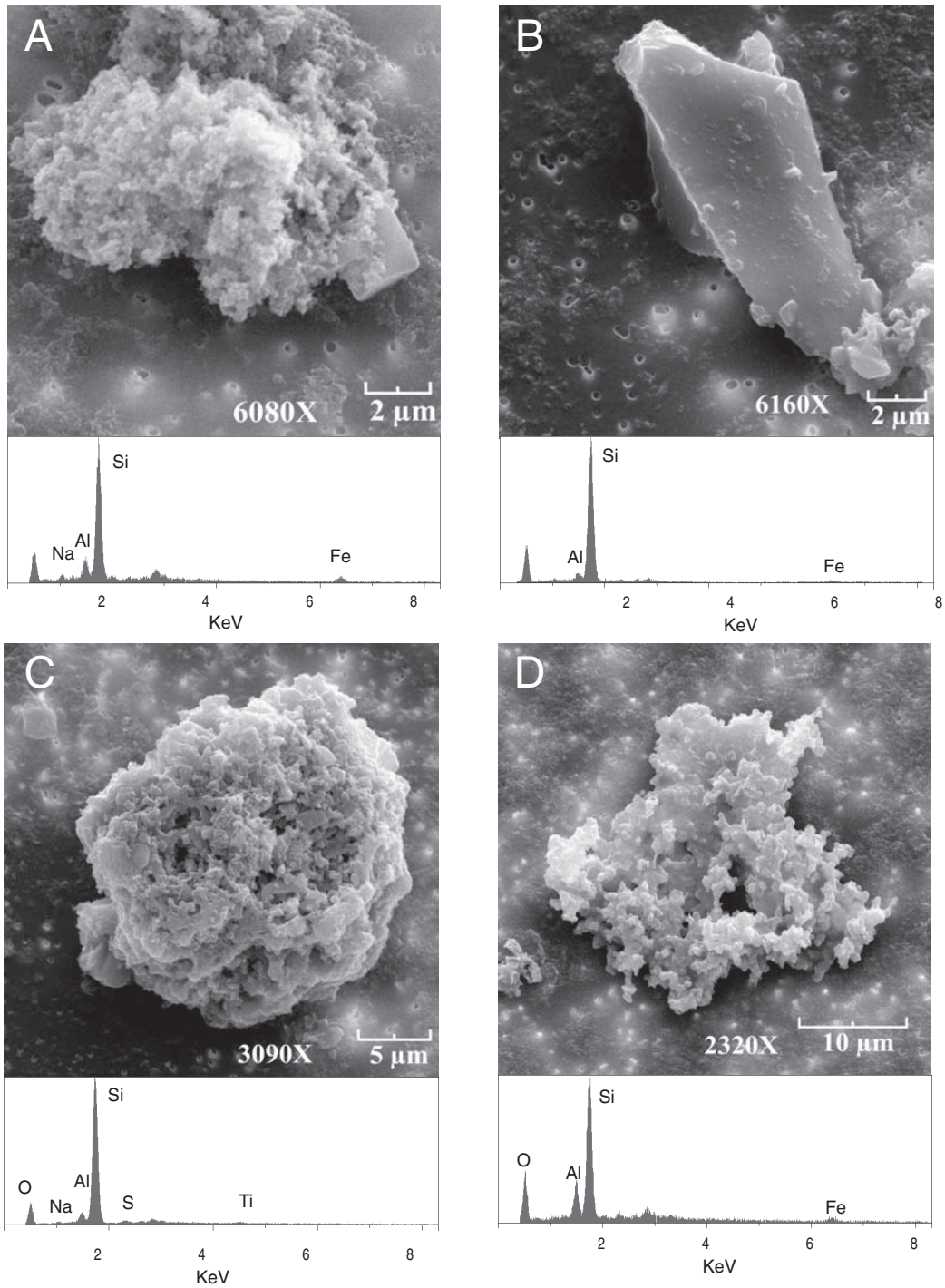

FIG. 6. Scanning electron microscope (SEM) images of leached and precipitated silica. A. Precipitated silica. This image shows silica that has been precipitated from solution. Note the soft amorphous edges of the image. B. Quartz shard. This shard must have been ejected from within the volcano into the hydrothermal fluid. C. Leached host rock. Silica is the only remaining component left behind after hot acid leaching. Soft edges and ball-like shape suggest that the particle was not fresh but had been tumbled by hydrothermal fluids. D. Leached rock. This particle is another remnant of the host rock left after acid leaching. It still retains some Al. The fine edges and delicate features suggest a very recently formed particle.

quartz and glass shards (Figs. 6B, 7C). Iron was present almost exclusively as freshly precipitated amorphous Fe oxyhydroxides (Fig. 8), whereas S was present as both sulfates (Figs. 7B, 9) and elemental S (Fig. 8). Aluminum was present predominantly as aluminum phosphate-sulfate minerals, including alunite group minerals [$(Na,K)\ Al_3(SO_4)_2(OH)_6$; Fig. 9] and woodhousite group minerals [$CaHAl(PO_4/SO_4)OH_6$]. The ratio of Al to S in spot analysis of individual crystals was ~1.5:1, suggesting that the predominant form of Al is alunite. Ca-, Na-, and K-rich particles were present both within the alunite group minerals and within clays, whereas Mg was associated only with clays. The elemental analyzer (IXRF) on the SEM is not extremely sensitive to P, however the P that could be detected was associated with the alunite crystals. It is possible that this P coprecipitated with the alunite, although the co-occurrence of Ca with the P suggests that the P is, in part, contained in woodhousite group minerals. It is also likely that a significant portion of the P coprecipitated onto fresh Fe oxyhydroxides (Feely et al., 1998).

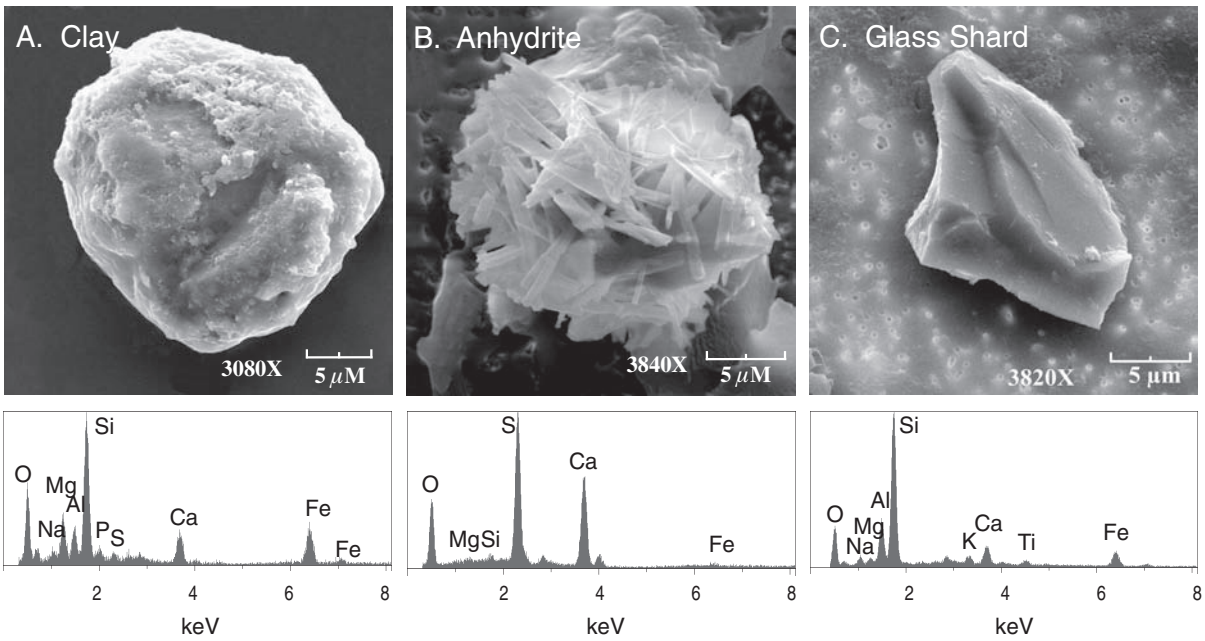

FIG. 7. Scanning electron microscope (SEM) images of minor particulate phases. Clay was regularly present throughout the particulate samples and was likely the main phase responsible for the observed Ca and Mg values. Anhydrite and glass shards were present but their occurrence was rare.

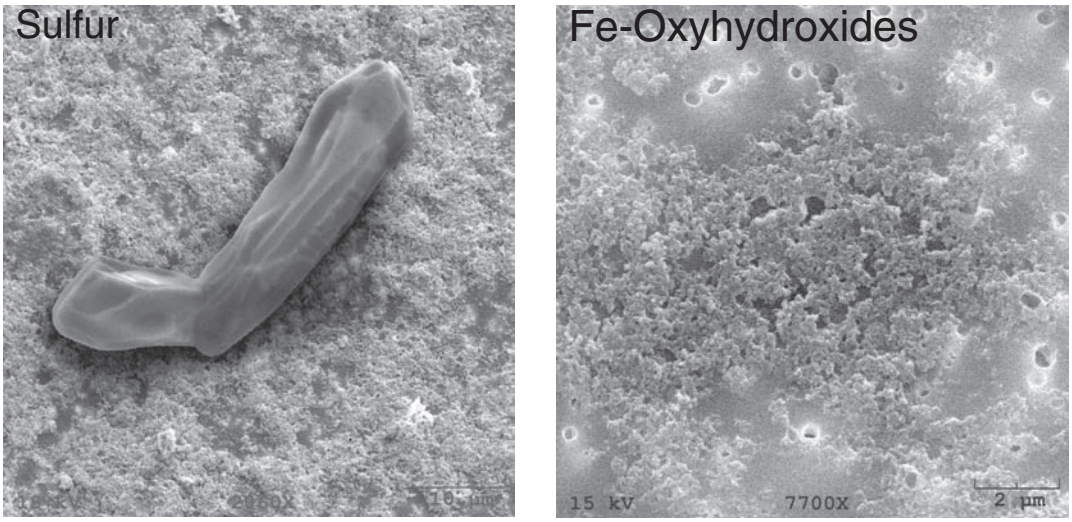

FIG. 8. Scanning electron microscope (SEM) images of two major particle types from the upper plume. The particulate matter above the volcano was composed primarily of elemental sulfur, Fe oxyhydroxides, and alunite. An example of a particle of elemental sulfur is shown in the left panel. Fe oxyhydroxides are shown in the right panel. Alunite is shown in Figure 9.

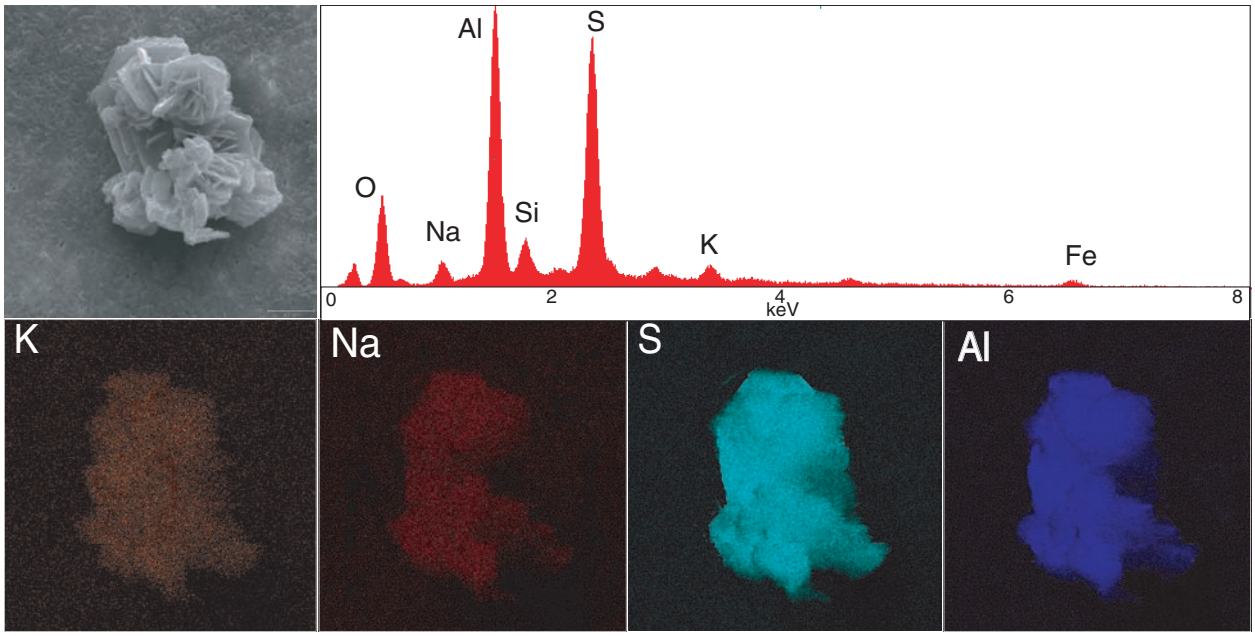

FIG. 9. Element mapping of an alunite crystal found in the hydrothermal plume above NW Rota volcano. The gray scale image is the SEM image. The remaining colored images are elemental maps of the elements indicated. The graph next to the SEM image is a spot X-ray analysis of the particle. The bulk XRF data show significant amounts of Ca and P (Table 1). Our SEM data show that Ca and some of the P are associated with the alunite phase. Because the mapped signals from the P and Ca are faint, those data are not shown due to the difficulty in viewing them.

In the lower plume, numerous elemental phases are greatly reduced when compared to the upper plume (Fig. 5, Tables 1–3). We observe a similar magnitude of total dissolvable Mn ($Mn_{(total\ dissolvable)}$) in both plumes with the maximum value in the upper plume 1.6× greater than the maximum Mn in the lower plume. Total dissolvable Fe ($Fe_{(total\ dissolvable)}$) is enriched 5× in the upper versus the lower plumes. Other elements in the particulate phase are variably enriched from ~3 to ~12× greater in the upper versus lower plumes, except for S which is ~70× more enriched in the upper plume. This enrichment in particulate S is responsible for a ~90× enrichment in ΔNTU in the upper plume versus the lower plume.

Total and dissolved metals: Dissolved Fe and Mn are common indicator elements for hydrothermal activity and were elevated in the plumes at NW Rota-1. The level of Fe in the upper plume was extremely elevated when compared to background seawater. Dissolved Fe from hydrothermal systems is typically in the Fe^{2+} state and is oxidized to Fe^{3+} within several hours (Field and Sherrell, 1999), and the Fe^{3+} rapidly forms Fe oxyhydroxide particles (Fig. 8). Thus, as the water ages, a greater percentage of the Fe is in the particulate phase. Most of the Fe in the plumes at NW Rota-1 is in the particulate phase, with particulate Fe ranging from 60 to 90 percent of the $Fe_{(total\ dissolvable)}$ and averaging ~73 percent. By contrast, Mn is transformed into the particulate phase much more slowly (months to years: Cowen et al., 1990). At NW Rota-1 particulate Mn is 0.1 percent of the $Mn_{(total\ dissolvable)}$.

Dissolved gases and acidity: The samples from the hydrothermal plumes show significant additions of CH_4, ^3He, CO_2, and S and decreases in pH (Table 2). The CH_4 values observed here (~4 nM) are enriched over background seawater by a factor of ~4×, which is comparable to the levels observed along the midocean ridges. The ^3He in the plumes is extraordinarily elevated. We observe a similar magnitude of ^3He in both plumes, with the maximum value in the upper plume 2.8× greater than the maximum ^3He in the lower plume. The ^3He has a mantle source and its enrichment in the plumes indicates the unequivocal presence of mantle gasses (Craig and Lupton, 1981). Significant decreases in pH observed in the plume (Figs. 3, 4) correlate well with increases in CO_2 (Fig. 10). Decreases in pH are caused both by the addition of CO_2 and mineral acidity (H^+), and at typical seawater alkalinities the addition of equal amounts of CO_2 or H^+ will decrease the pH of seawater by an approximately equal amount unit. When CO_2 is added to seawater ΣCO_2 values increase, but when mineral acidity is added to seawater ΣCO_2 stays constant. By measuring both pH and ΣCO_2 we can assess the contributions of both mineral acidity and CO_2. The plot of the increase in ΣCO_2 versus change in pH (Fig. 10) reveals two trends, one with a slope of ~360 and the other with a slope of ~65. The slope of ~360 is solely due to the addition of CO_2 to the plumes, whereas the slope of ~65 must be the result of the addition of both mineral acidity and CO_2. This trend line indicates that ~20 percent of the pH change is due to CO_2 with the remaining ~80 percent from mineral acidity. The samples with both mineral acidity and CO_2 come from the plume at shallower depths, whereas the samples with only CO_2 are those found in the deeper plume.

Discussion

The largest chemical enrichments above background seawater in the hydrothermal plumes observed above NW Rota-1 volcano are for the magmatic volatiles CO_2 and SO_2. The input of CO_2 and SO_2 cause a measurable decrease in the pH

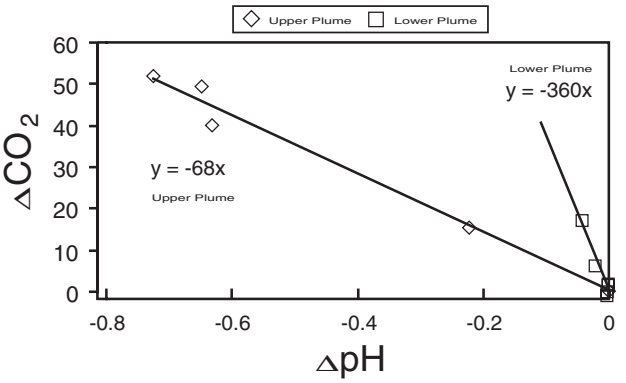

FIG. 10. Plot showing the influence of CO_2 gas on the pH of seawater above NW Rota-1 (change in total CO_2 (ΔCO_2) vs. change in pH (ΔpH). Decreases in the pH of seawater are caused by the addition of mineral acidity and/or the addition of CO_2. The addition of CO_2 increases ΔCO_2 and decreases pH while the addition of acid decreases pH and ΔCO_2 remains constant. When only CO_2 is added, the slope of CO_2 vs. pH is $\approx$ 360. The samples in the upper plume fall along a line with slope = 65, which shows that 20 percent of the pH change comes from the addition of CO_2 and the balance from the addition of acid. The samples in the lower plume fall along the line of CO_2 addition, only suggesting that there is no mineral acidity added to these waters.

of ambient seawater. The plumes are also enriched with a variety of other chemical components at 100s to 1,000s × above their levels in ambient seawater. The net chemical signature of these plumes is distinctly different from those associated with typical midocean ridge hydrothermal activity. In particular, Al has not been observed at levels greater than ~10 nM in hydrothermal plumes found in most settings. The plumes observed at NW Rota-1 have particulate Al levels >1,000 nM, comparable to the levels observed for dissolved Al in the Manus basin (Gamo et al., 1993) and in the particulate form at Brothers Seamount on the Kermadec arc (de Ronde et al., 2005). The particulate Al observed here is present predominantly as alunite, a mineral that is common to settings of intense leaching of volcanic rocks by sulfurous and sulfuric acids responsible for advanced argillic alteration.

Sulfur, carbon, and acidity

If the source fluid in the plume is diluted with ambient seawater by a factor of 1,000 to 10,000, it can be estimated that these fluids for the plumes must have had $[H^+] \approx 200$ to 2,000 mM or a pH range from 0 to 0.7. Thus, even a conservative estimate of fluid dilution indicates that these fluids were extraordinarily acidic (1,000× dilution yields pH $\approx$ 0.7), which is lower than the value of 2.0 found by Embley et al. (2006). The presence of alunite and elemental S suggests that much of this mineral acid is sulfuric acid. Sulfuric acid in hydrothermal systems is formed from volcanic SO_2 released to the hydrothermal system, which reacts with water and forms H^+ following one of the reactions below:

$$4SO_2 + 4H_2O = H_2S + 3H_2SO_4, \quad (1)$$

$$SO_2 + H_2O = HSO_3^- + H^+, \quad (2)$$

and

$$3SO_2 + 2H_2O = S_{(S)} + 2H_2SO_4. \quad (3)$$

The absence of H_2S in the plumes suggests that reaction 1 is not an important chemical reaction at this volcano. Although H_2S can be oxidized quickly (within hours) in hydrothermal plumes, the presence of the plume very near the summit of the volcano and the presence of dissolved Fe (~30%) suggest that the sampled fluids were only recently vented. The SEM analyses of the particles revealed no metal sulfides, suggesting that metal sulfide formation was not responsible for removing the H_2S from the vented waters. The absence of H_2S and metal sulfides in the plume also suggests that it is a minor component in the vented fluids. Reaction 2 is considered the most likely first step when magmatic gasses rich in SO_2 come in contact with water. When this volcano was revisited in 2006, $SO_{2(aq)}$ and HSO_3^- were detected in the plumes found at that time (B. Takano, 2006, pers. commun.). The presence of elemental S (Table 2, Figs. 3, 4) in the plumes suggests that reaction 3 is also important. This is supported by ROV dives to NW Rota-1 that found a small eruptive crater just below the summit of the volcano actively expelling aqueous fluids and large amounts of liquid and solid elemental S which coated the ROV (Embley et al., 2006; Chadwick et al., in prep.).

Magmatic fumaroles and condensates on subaerial volcanoes generally contain both sulfuric (SO_4^{2-}) and hydrochloric (HCl) acids (Symonds et al., 1994, and references therein), implying that acidity is likely generated by a mixture of these two acids. Symonds et al. (1994) and Hedenquist (1995) show that, in general, S exceeds Cl by a factor of 2 or more for subaerial arc volcanoes. The data presented here cannot differentiate between acid produced by SO_2 and HCl, but the presence of alunite and native S and the comparison with subaerial examples suggest that both acids may be contributing to the total mineral acidity ($[H^+] = 217\ \mu M$). If we assume an S/Cl ratio from 1:1 to 2:1 and that each SO_2 and HCl produce 2 H^+ and 1 H^+, respectively, then the total amount of SO_2 producing the mineral acidity falls in the range ~72 to ~87 μM (or ~144 to ~174 μM H^+) with the balance of acid, ~43 to ~73 μM, coming from HCl. From this, and our measured value of 50 μM CO_2, we estimate that S + Cl is 2 to 4 × greater than CO_2. This is consistent with gases emitted from many subaerial volcanoes along convergent plate boundaries where (S + HCl):$CO_2 \geq 1$ (see summary by Toutain, 1991; Symonds et al., 1994; and Taran et al., 1995).

At NW Rota-1, we estimate S/C to be in the range from 1.4 to 1.7:1, at the high end of the range observed at subaerial arc volcanoes. The range for NW Rota-1 may be higher than we measured because milky white plumes at the vent site observed by Embley et al. (2006) are thought to be created by the formation of elemental S, all of which may not be carried upward into the plumes sampled by us. The use of acidity to calculate SO_2 content is also an underestimate because the precipitation of elemental sulfur from SO_2 and H_2S does not produce acid.

CO_2 and ^{3}He

Whereas ^{3}He is almost entirely from a mantle source, CO_2, ^{4}He, and S can have other sources, including oceanic crust, sedimentary carbonates, and organic matter (e.g., de Hoog et al., 2001). The helium isotope values in the plumes at NW Rota-1 have an $R/R_a = 8.43 \pm 0.09$, which is within the generally accepted upper mantle value of 8.0 ± 1 (Poreda and Craig, 1989). The helium coming out of subduction zone

volcanoes is a mixture of helium from the melting of the mantle and helium from the subducting slab. The subducting slab retains little of its original ^{3}He and is therefore relatively richer in ^{4}He. This has the effect of decreasing the R/R_a of arc helium to ~5 to ~7 R/R_a (Sano and Marty, 1995). Gases from submarine arc volcanoes have variable R/R_a (8.1 at Suiyo seamount on the Izu-Bonin arc: Tsunogai et al., 1994; 7.31 at NW Eifuku seamount on the Mariana arc: Lupton et al., 2006; 5.9–7.4 at Brothers Volcano on the Kermadec arc: de Ronde et al., 2005).

The ratio of CO_2 to ^{3}He at NW Rota-1 ($3.25 \pm 0.07 \times 10^9$) is elevated when compared to the accepted midocean ridge value of 2×10^9, but well within the range for midocean ridge hydrothermal fluids ($0.7–4.6 \times 10^9$) and basaltic glasses ($0.2–7.5 \times 10^9$; see Resing et al., 2004, and references therein). By comparison, 3.25×10^9 is considerably lower than the values observed at other submarine arc volcanoes (12×10^9 at Suiyo seamount: Tsunagai et al., 1994; 20×10^9 at NW Eifuku seamount: Lupton et al., 2006), and in a wide range of volcanic gasses at subaerial arc volcanoes (~6 to ~34 $\times 10^9$: Sano and Marty, 1995, and references therein). These data suggest that the source of both the ^{3}He and the CO_2 observed here is MORB-like and predominantly from the upper mantle with little contribution from the slab. If we use the approach of Sano and Marty (1995) and Fischer et al. (1998), we calculate that ~38 percent ($[3.25 \times 10^9–2.0 \times 10^9]/[3.25 \times 10^9] = 38\%$) of the CO_2 venting here comes from a nonmantle source. However, the $CO_2/^3$He ratio at NW Rota falls within the global midocean ridge value, making it difficult to invoke a slab carbon component.

NW Rota-1 is located on the back-arc side (western end) of a chain of cross-arc volcanoes. Compared to volcanoes directly on the arc, this location places the volcano at an intermediate position with respect to the subducting slab and the back-arc spreading center. The high magnesium mafic lavas observed at another of the cross chain volcanoes, Chaife, located 25 km east-northeast of NW Rota-1, are interpreted as originating from adiabatic melting of an anhydrous portion of mantle wedge (Kohut et al., 2006). However, because NW Rota is closer to the arc than to the back arc, it may have erupted more slab-influenced volatiles in the past.

Acid-sulfate alteration

Leaching of Al^{3+}, $Fe^{2+,3+}$, Na^+, K^+, and other cations from the volcanic rocks at NW Rota is evident in many of the Si- and Al-rich phases found suspended in the plume. One class of particles appears to be particles of leached volcanic rock (Fig. 6C-D), which are clearly distinct from both reprecipitated Si (Fig. 6A) and quartz (Fig. 6B). These remnants are the equivalent of the "vuggy silica" found in areas of acidic alteration on subaerial volcanoes (e.g., Cooke and Simmons, 2000).

Where hot acidic fluids continue to dissolve the rock, greatly increasing the concentration of dissolved solids, the solutions eventually become saturated, whereupon increases in pH or decreases in temperature cause mineral precipitation. In particular, Al that has been liberated by the sulfuric acid combines with sulfate to form $Al_2(SO4)_3$ phases from alunite ($KAl_3(SO_4)_2(OH)_6$) to natroalunite Na ($NaAl_3(SO_4)_2(OH)_6$; Fig. 9). The Al-rich plumes observed in the Manus basin and at Brothers volcano on the Kermadec arc are hypothesized to have arisen from the venting of sulfuric acid-rich fluids (Gamo et al., 1993; de Ronde et al., 2005). Rock samples from Brothers submarine volcano (de Ronde et al., 2005) and Conical seamount (Petersen et al., 2002; Gemmell et al., 2004) revealed alunite and other phases consistent with advanced argillic alteration on the sea floor. The Al phases identified by SEM in the plume samples from NW Rota show that it is present primarily as a sulfate with varying amounts of Na and K. Aluminum is also present in much smaller amounts as clays (Fig. 7A), leached Al silicates (Fig. 6D), and other precipitates (Fig. 6A). In addition to leached volcanic rock (e.g., vuggy silicates) and alunite, elemental S was also abundant within the plumes (Table 2, Fig. 8A). The mechanism responsible for this would appear to be the direct venting of SO_2-rich fluids into ambient seawater (reaction 3).

The stripping of cations from the host rock by sulfurous acids may also be reflected in the elevated Fe/Mn ~16:1 ratios found in the whole-water subsamples ($Fe_{(total\ dissolvable)}$ and $Mn_{(total\text{-}dissolvable)}$) from the plumes. Fe/Mn ratios found in typical midocean ridge hydrothermal fluids range from ~1:1 to ~5:1 (e.g., Von Damm et al., 1990, and references therein), whereas elevated Fe/Mn ratios have been observed in CO_2-rich hydrothermal systems (e.g., 30:1 at Loihi: Sedwick et al., 1992) and where shoreline lava flows enter the ocean from the Kilauea volcano (54:1: Resing et al., 2002). Resing et al. (2002) attributed the elevated Fe/Mn ratios to the congruent dissolution of the host rock by highly acidic fluids generated by the interaction of lava with seawater. Although elevated, the Fe/Mn ratio observed at NW Rota-1 is still less than that of the host rock (e.g., BHVO and AGV-1: Govindaraju, 1989). This may reflect the removal of Fe from the fluids as Fe sulfide. Alternatively, Massoth et al. (2004) observed a similar Fe/Mn ratio at the Brothers volcano on the Kermadec arc and suggested this ratio might be indicative of magmatic fluids (e.g., typical of fluid inclusions hosted by some magmatic hydrothermal ore deposits).

Particulate phosphorous and vanadium

Feely et al. (1998) demonstrated that P/Fe ratios in particulate matter in plumes above midocean ridge hydrothermal systems range from 0.06:1 to 0.3:1 and reflect scavenging of dissolved phosphate from ambient waters. Based on local phosphate levels of 1.8 to 2.5 μM at 400- to 500-m depth in this area (Sabine et al., 1999), particulate P/Fe ratios here should be close to 0.1:1 and certainly <0.15:1. However, the ratio we observe in the upper plume at NW Rota is 0.55:1, suggesting that most of the particulate P is not scavenged from the local seawater but instead arises from the volcano. The SEM data support this conclusion because the observed particulate P is mostly associated with alunite phases [e.g., woodhousite, $CaHAl(PO_4/SO_4)OH_6$] and only partly associated with the Fe oxyhydroxides. This conclusion is further supported by the association of particulate Ca with the alunite phases. The lower plume has a ratio of 0.36:1, which is closer to, but still higher than, the expected ratio for scavenging of P from seawater by Fe. The lower plume ratio probably reflects less P exiting the hydrothermal system. The ratio of Al/Mn is much lower in the lower plume than in the upper plume (Fig. 5), suggesting that P-bearing alunite is being retained within the system.

At midocean ridges, V, like P, is scavenged from ambient seawater and only has a small hydrothermal or volcanic source. P is preferentially scavenged over V by Fe oxyhydroxides. Feely et al. (1998) found that particulate V/Fe ranged from 0.0026 to 0.0045 in plumes above midocean ridges and was inversely correlated with dissolved P. This competitive scavenging results in plumes with elevated phosphate having particles with lower V/Fe ratios. The particulate V/Fe ratio in the upper plume at NW Rota-1 is 0.0026, at the low end of the range for midocean ridge plumes, and suggests that the excess volcanic P competitively occupies sites on the Fe oxyhydroxide particles at the expense of the V. The V/Fe ratio is higher in the lower plume, reflecting the smaller contribution of magmatic P and lower P/Fe ratio in the lower plume. We suggest that particulate V in the plumes is largely scavenged from local ambient seawater by the hydrothermal Fe, with a minimum contribution from the magmatic-hydrothermal system.

The addition of volcanic P might play an important role in enhancing the use of hydrothermal Fe as a trace nutrient in the surface ocean (e.g., Wells et al., 1999). The addition of any P and Fe to the surface ocean probably enhances productivity, however, the P/Fe ratio of these particles (0.55:1) is much lower than that of oceanic plankton (P/Fe ≈ 133: Ho et al., 2003), suggesting that P rather than Fe could limit primary productivity if the fluids of the type observed here were vented into the surface ocean. Finally, the use of P/Fe ratios in sediments as a paleoindicator of oceanic P also could be problematic.

The lower plume

The chemical data presented here show two distinct plumes and therefore two plume sources. The upper plume is rich in mineral acidity, CO_2, Al as alunite, elemental S, and leached and precipitated silicates. The lower plume, meanwhile, retains a strong Mn, ^{3}He, and Fe signal but many components found in the upper plume are absent, most notably alunite, elemental and sulfate S, and mineral acidity.

The origin of the fluids feeding the lower plume may be the same as those exiting from the pit site. However, instead of exiting the volcano they rise through the edifice and continue to react with the host rock and mix with ambient seawater (e.g., Fig. 11). As this happens, the remaining mineral acidity is consumed and the fluids approach equilibrium with the rock and much of the dissolved solids precipitate. Mn is fairly soluble within hydrothermal systems and ^{3}He is conservative with no removal process. Figure 5 shows that as the fluids

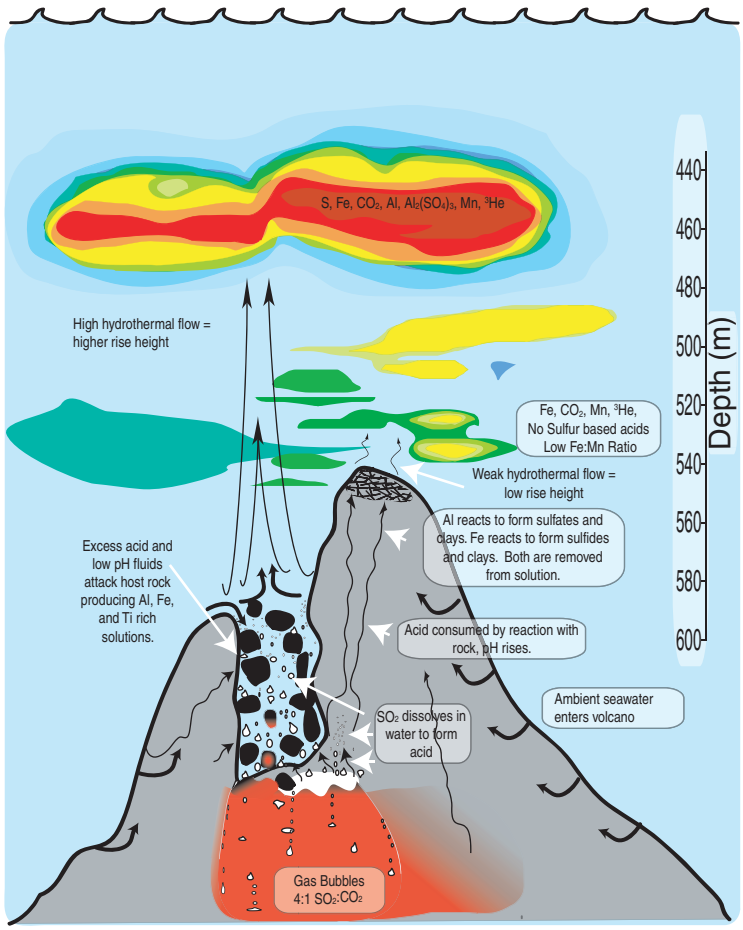

FIG. 11. Schematic diagram shows some of the processes occurring on NW Rota-1 volcano. A deeper more active pit is forcefully ejecting hot buoyant hydrothermal fluids into the ambient water column. These fluids rise over 100 m above the volcano. Hydrothermal activity at the summit is more diffuse, producing fluids that do not rise as high into the water column.

continue to react they gain additional Mn. These processes result in a lower Fe/Mn ratio and decreases in Al S, Si, and other trace components relative to Mn in the fluids exiting the volcano at this depth.

Conclusions

In 2003, NW Rota-1 was vigorously venting extremely acidic, S rich hydrothermal fluids. These fluids stripped cations, most notably Al, from the host rocks. The fluids were then vented at the sea floor, forming plume waters rich in elemental S, alunite, leached silicates, CO_2, and particulate Fe. Helium isotope data, $CO_2/^3He$ ratios, and changes in CO_2 with respect to pH indicate that the volcano was venting mantle gasses and fluids rich in SO_2. The helium isotopes and $CO_2/^3He$ are MORB-like, possibly reflecting the location of the volcano west of the arc front and closer to the back arc. The abundance of S, acid, and Al are consistent with conditions typical of high-sulfidation environments which are characterized by the presence of alunite minerals and advanced argillic alteration (e.g., Heald et al., 1987; Sillitoe et al., 1996).

Resing and Sansone (1996) argued that hot acidic fluids of this type would react quickly with the host rocks, resulting in the consumption of most of the H^+ ions in exchange for cations. This process is consistent with the chemistry of the lower plume fluids. However, the more actively venting fluids forming the upper plume did not have time to react fully with the host rock. We conclude that the source of the acid must be very near the surface of the volcano. There are at least two possible explanations for this—the magma chamber is very shallow, resulting in a short reaction path and short reaction time, or magmatic fluids rich in SO_2 have risen from deep within the volcano and mixed with ambient water just below the surface of the volcano. These two situations are not mutually exclusive. Observations by Embley et al. (2006) and Chadwick et al. (in prep.) show that in 2004, 2005, and 2006, ~1 to ~3 yr after this study, NW Rota-1 was in an active state of eruption which supports the idea that a degassing magma chamber was very near the summit of the volcano.

The activity taking place at NW Rota is very robust, suggesting that the majority of fluids vent directly into the ocean. If the fluids escape the volcano at the pH observed here, the deposition of metals within the volcano is difficult, potentially producing what would be a "barren" mineral prospect. The escape of these mineral-laden fluids likely produces the upper plume (Fig. 11). By contrast, the fluids escaping from the unconsolidated debris at the summit of the volcano and producing the lower plume have little mineral acidity, relatively small amounts of Al, S, and much lower Fe/Mn. The acidity of these fluids must have been consumed within the volcano, which would result in the subsea-floor deposition of the dissolved mineral load otherwise lost by the fluid venting from the highly active crater.

Acknowledgments

We thank the Captain and crew of the *R/V Thompson* for their excellent support during the 2003 and 2004 SROF cruises. Andrew Graham conducted the methane analysis. We thank Sharon Walker for processing the optical backscatter data, constructive discussions, and for supporting this project in many ways. We thank Susan Merle for logistical and mapping support. Discussions with David Butterfield benefited this manuscript. Constructive reviews of this work were provided by Anthony Harris and Jacob Lowenstern. This project was funded by NOAA's Office of Ocean Exploration and the NOAA PMEL Vents Program. This publication was supported by the Joint Institute for the Study of the Atmosphere and Ocean (JISAO) under NOAA Cooperative Agreement NA17RJ1232 and is JISAO contribution 1308. This is Pacific Marine Environmental Laboratory contribution 2908.

February 22, 2006; October 10, 2007

REFERENCES

Bajnóczi, B., Seres-Hartai, É., and Nagy, G., 2004, Phosphate-bearing minerals in the advanced argillic alteration zones of high-sulphidation type ore deposits in the Carpatho-Pannonian region: Acta Mineralogica-Petrographica, Szeged, v. 45/1, p. 81–92.

Butterfield, D.A., Massoth, G.J., McDuff, R.E., Lupton, J.E., and Lilley, M.D., 1990, Geochemistry of hydrothermal fluids from Axial seamount hydrothermal emissions study vent field, Juan de Fuca Ridge: Subseafloor boiling and subsequent fluid-rock interaction: Journal of Geophysical Research, v. 95, p. 12,895–12,921.

Butterfield, D.A., McDuff, R.E., Mottl, M.J., Lilley, M.D., Lupton, J.E., and Massoth,G.J., 1994, Gradients in the composition of hydrothermal fluids from the Endeavour Segment vent field: Phase separation and brine loss: Journal of Geophysical Research, v. 99, no. B5, p. 9561–9583.

Chadwick, W.W., Jr., Cashman, K.V., Embley, R.W., Dziak, R.P., De Ronde, C.E.J., Matsumoto, H., Deardorff, N., and Merle, S.M., 2007, Direct video and hydrophone observations of submarine explosive eruptions at NW Rota-1 volcano, Mariana arc: Journal of Geophysical Research, in press.

Cheminée, J.-L., Stoffers, P., McMurtry, G., Richnow, H., Puteanus, D., and Sedwick, P., 1991, Gas-rich submarine exhalations during the 1989 eruption of Macdonald Seamount: Earth and Planetary Science Letters, v. 107, p. 318–327.

Cooke, D.R., and Simmons, S.F., 2000, Characteristics and genesis of epithermal gold deposits: Reviews in Economic Geology, v. 13, p. 221–244.

Cowen, J.P., Massoth, G.J., and Feely, R.A., 1990, Scavenging rates of dissolved manganese in a hydrothermal vent plume: Deep Sea Research, v. 37, p. 1619–1637.

Craig, H., and Lupton, J., 1981, Helium-3 and mantle volatiles in the ocean and the ocean crust, *in* Emiliani, C.E., ed., The sea: New York, J. Wiley, New York, v. 7, p. 391–428.

de Hoog, J.C.M., Taylor, B.E., and van Bergen, M.J., 2001, Sulfur isotope systematics of basaltic lavas from Indonesia: Implications for the sulfur cycle in subduction zones: Earth and Planetary Science Letters, v. 189, p. 237–252.

de Ronde, C.E.J., et al., 2005, Evolution of a submarine magmatic-hydrothermal system: Brothers volcano, southern Kermadec arc, New Zealand: Economic Geology, v. 100, p. 1097–1133.

Deyell, C.L., Rye, R.O., Landis, G.P., and Bissig, T., 2005, Alunite and the role of magmatic fluids in the Tambo high-sulfidation deposit, El Indio-Pascua belt, Chile: Chemical Geology, v. 215, p. 185–218.

Dill, H.G., 2001, The geology of aluminum phosphates and sulphates of the alunite group minerals: A review: Earth Science Review, v. 53, p. 35–93.

Embley, R.W., Chadwick, W.W. Jr., Baker, E.T., Butterfield, D.A., Resing, J.A., de Ronde, C.E.J., Tunnicliffe, V., Lupton, J.E., Juniper, S.K., Rubin, K.H., Stern, R.J., Lebon, G.T., Nakamura, K.-I., Merle, S.G., Hein, J.R., Wiens, D.A., and Tamura, Y., 2006, Long-term eruptive activity at a submarine arc volcano: Nature, v. 441, no. 7092, p. 494–497

Embley, R.W., Baker, E.T., Chadwick, W.W., Jr., Lupton, J.E., Resing, J.A., Massoth, G.L., and Nakamura, K., 2004, Explorations of Mariana arc volcanoes reveal new hydrothermal systems [abs.]: EOS, v. 85, no. 4, p. 37, 39.

Feely, R.A., Massoth, G.J., and Lebon, G.T., 1991, Sampling of marine particulate matter and analysis by X-ray fluorescence spectrometry: Geophysical Monograph Series, v. 63, p. 251–257.

Feely, R.A., Trefry, J.H., Lebon, G.T., and German, C.R., 1998, The relationship between P/Fe and V/Fe ratios in hydrothermal precipitates and dissolved phosphate in seawater: Geophysical Research Letters, v. 25, p. 2253–2256.

Field, M.P., and Sherrell, R.M., 2000, Dissolved and particulate Fe in a hydrothermal plume at 9° 45'N, East Pacific Rise: Slow Fe (II) oxidation

kinetics in Pacific plumes: Geochimica et Cosmochimica Acta, v. 64, p. 619–628.

Gamo, T., Sakai, H., Ishibashi, J., Nakayama, E., Isshiki, K., Matsuura, H., Shitashima, K., Takeuchi, K., and Ohta, S., 1993, Hydrothermal plumes in the eastern Manus basin, Bismarck Sea: CH_4, Mn, Al, and pH anomalies: Deep Sea Research, v. 40, p. 2,335–2,349.

Gamo, T., Okamura, K., Charlou, J-L., Urabe, T., Auzende, J-M., Ishibashi, J., Shitashima, K., and Chiba, H., 1997, Acidic and sulfate-rich fluids from the Manus back-arc basin, Papua New Guinea: Geology, v. 25, p. 139–142.

Gemmell, J.B., Binns, R.A., and Parr, J.M., 1999, Characterization of submarine, high sulphidation alteration, Desmos, caldera, eastern Manus basin, Papua New Guinea [abs.]: Fifth Biennial SGA Meeting and the Tenth Quadrennial IAGOD Symposium, London, August 1999, Abstracts, v. 1, p. 503–506.

Gemmell, J.B., Sharpe, R., Jonasson, I.R., and Hezig, P.M., 2004, Sulfur isotope evidence for magmatic contributions to submarine and subaerial gold mineralization: Conical seamount and the Ladolam gold deposit, Papua New Guinea: Economic Geology, v. 99, p. 1711–1725.

Govindaraju, K., 1989, 1989 compilation of working values and sample description for 272 geostandards: Geostandards Newsletter, v. 13, p. 1–113.

Heald, P., Foley, N.K., and Hayba, D.O., 1987, Comparative anatomy of volcanic-hosted epithermal deposits: Acid-sulfate and andularia-sercite types: Economic Geology, v. 82, p. 1–26.

Hedenquist, J.W., 1995, The ascent of magmatic fluid: Discharge versus mineralization: Mineralogical Association of Canada Short Course Volume 23, p. 263–289.

Hedenquist, J.W., Aoki, M., and Shinohara, H., 1994, Flux of volatiles and ore forming metals from the magmatic-hydrothermal system of Satsuma Iwojima volcano: Geology, v. 22, p. 585–588.

Hedenquist, J.W., Arribas, R., and Gonzalez-Urien, E., 2000, Exploration for epithermal gold deposits: Reviews in Economic Geology, v. 13, p. 245–277.

Herzig, P.M., Hannington, M.D., and Arribas, A., Jr., 1998, Sulfur isotopic composition of hydrothermal precipitates from the Lau back-arc: Implications for magmatic contributions to seafloor hydrothermal systems: Mineralium Deposita, v. 33, p. 226–237.

Ho, T-Y., Quigg, A., Finkel, Z.V., Milligan, A.J., Falkowski, P.G., and Morel, F.M.M., 2003, The elemental composition of some marine phytoplankton: Journal of Phycology, v. 39, p. 1145–1159.

Kohut, E.J., Stern, R.J., Kent, A.J.R., Nielsen, R.L., Bloomer, S.H., and Leybourne, M., 2006, Evidence for adiabatic decompression melting in the southern Mariana arc from high-Mg lavas and melt inclusions: Contributions to Mineralogy and Petrology, v. 152, p. 201–221.

Lewis, E., and Wallace, D., 1998, Program developed for CO_2 system calculations: Oak Ridge, Tennessee, Carbon Dioxide Information Analysis Center, U.S. Department of Energy, Report ORNL/CDIAC-105.

Lupton, J., Butterfield, D., Lilley, M., Evans, L., Nakamura, K.-I., Chadwick, W., Jr., Resing, J., Embley, R., Olson, E., Proskurowski, G., Baker, E., de Ronde, C., Roe, K., Greene, R., Lebon, G., and Young, C.O., 2006, Submarine venting of liquid carbon dioxide on a Mariana arc volcano: Geochemistry, Geophysics, Geosystems, v. 7, Q08007, doi: 10.1029/2005GC001152.

Lupton, J.E., Delaney, J.R., Johnson, H.P., and Tivey, M.K., 1985, Entrainment and vertical transport of deep-ocean water by hydrothermal plumes: Nature, v. 316, p. 621–623.

Massoth, G.J., de Ronde, C.E.J., Lupton, J.E., Feely, R.A., Baker, E.T., Lebon, G.T., and Maenner, S.M., 2004, The chemically rich and diverse submarine hydrothermal plumes of the southern Kermadec volcanic arc (New Zealand): Geological Society of London Special Publication 219, p. 119–139.

McMurtry, G.M., Sedwick, P.N., Fryer, P., Vonderhaar, D.L., and Weh, H.W., 1993, Unusual geochemistry of hydrothermal vents on submarine arc volcanoes: Kasuga Seamounts northern Mariana arc: Earth Planetary Science Letters, v. 114, p. 517–528.

Measures, C.I., Yuan, J.C., and Resing, J., 1995, Determination of iron in seawater by flow injection analysis using in-line preconcentration and spectrophotometric detection: Marine Chemistry, v. 50, p. 3–12.

Millero, F.J., 1979, The thermodynamics of the carbonate system in seawater: Geochimica et Cosmochimica Acta, v. 43, p. 1651–1661.

Ocean Drilling Program Shipboard Scientific Party, 2001, Leg 193 Preliminary report: Anatomy of an active felsic-hosted hydrothermal system, eastern Manus basin: College Station, TX, Ocean Drilling Program, 97 p.

Peacock, S.M., 1990, Fluid processes in subduction zones: Science, v. 248, p. 329–337.

Peate, D.W., and Pearce, J.A., 1998, Causes of spatial compositional variations in Mariana arc lavas: Trace element evidence: The island arc, v. 7, p. 479–495.

Petersen, S., Herzig, P.M., Hannington, M.D., Jonasson, I.R., and Arribas, A. Jr., 2002, Submarine gold mineralization near Lihir Island, New Ireland fore-arc, Papua New Guinea: Economic Geology, v. 97, p. 1795–1813.

Poreda, R., and Craig, H., 1989, Helium isotope ratios in Circum Pacific volcanic arcs: Nature, v. 338, p. 473–478.

Resing, J.A., and Mottl, M.J., 1992, Determination of manganese in seawater by flow injection analysis using online preconcentration and spectrophotometric detection: Analytical Chemistry, v. 64, p. 2682–2687.

Resing, J.A., and Sansone, F.J., 1996, Al and pH anomalies in the Manus basin: Reappraised: Comments on the paper by T. Gamo et al., "Hydrothermal plumes in the eastern Manus basin, Bismarck Sea: CH_4, Mn, Al and pH anomalies": Deep Sea Research I, v. 43, p. 1867–1872.

——2002, The chemistry of lava-seawater interactions II: The elemental signature: Geochimica et Cosmochimica Acta, v. 66, p. 1925–1941.

Resing, J.A., Lupton, J.E., Feely, R.A., and Lilley, M.D., 2004, CO_2 and ^3He in hydrothermal plumes: Implications for mid-ocean ridge CO_2 flux: Earth and Planetary Science Letters, v. 226, p. 449–464.

Sabine, C.L., Key, R.M., Hall, M., 1999, Carbon dioxide, hydrographic, and chemical data obtained during the R/V *Thomas G. Thompson* cruise in the Pacific Ocean: Oak Ridge, Tennessee, Carbon Dioxide Information Analysis Center, U.S. Department of Energy, Report NDP-071.

Sakamoto-Arnold, C., Johnson, K., and Beehler, 1986, Determination of hydrogen sulfide in seawater using flow injection analysis and flow analysis: Limnology and Oceanography, v. 31, p. 894–900.

Sano, Y., and Matry, B., 1995, Origin of carbon in fumarolic gas from island arcs: Chemical Geology, v. 119, p. 265–274.

Sedwick, P.N., McMurtry, G.M., and Macdougall, J.D., 1992, Chemistry of hydrothermal solutions from Peles vents, Loihi seamount, Hawaii: Geochimica et Cosmochimica Acta, v. 56, p. 3643–3667.

Sillitoe, R.H., Hannington, M.D., and Thompson, F.H., 1996, High-sulfidation in the volcanogenic massive sulfide environment: Economic Geology, v. 91, p. 204–212.

Stern, R.J., Basu, N.K., Kohut, E., Hein, J., and Embley, R.W., 2004. Petrology and geochemistry of igneous rocks collected in association with ROV investigations of three hydrothermal sites in the Mariana arc: NW Rota-1, E. Diamante, and NW Eifuku [abs.]: EOS, Supplement v. 85, Abstract V43F-07.

Stoffregen, R., 1987, Genesis of acid-sulfate alteration and Au-Cu-Ag mineralization at Summitville, Colorado: Economic Geology, v. 82, p. 1575–1591.

Symonds, R.B., Rose, W.I., Bluth, G.J.S., and Gerlach, T.M., 1994, Volcanic gas studies: Methods, results and applications: Reviews in Mineralogy, v. 30, p. 1–66.

Taran, Y.A., Hedenquist, J.W., Korzhinsky, M.A., Tkachenko, S.I., and Shmulovich, K.I., 1995, Geochemistry of magmatic gases from Kudryavy volcano, Iturup, Kuril Islands: Geochimica et Cosmochimica Acta, v. 59, p. 1749–1761.

Tedesco, D., and Toutain, J.P., 1991, Chemistry and emission rate of volatiles from White Island volcano (New Zealand): Geophysical Research Letters, v. 18, p. 113–116.

Tsunogai, U., Ishibashi, J., Wakita, H., Gamo, T., Watanabe, K., Kajimura, T., Kanayama, S., and Sakai, H., 1994, Peculiar features of Suiyo seamount hydrothermal fluids, Izu-Bonin arc: Differences from subaerial volcanism: Earth and Planetary Science Letters, v. 126, p. 289–301.

Van der Hilst, R., Engdahl, R., Spakman, W., and Nolet, G., 1991, Tomographic imaging of subducted lithosphere below northwest Pacific island arcs: Nature, v. 353, p. 37–42.

Von Damm, K.L., 1990, Seafloor hydrothermal activity: Black smoker chemistry and chimneys: Annual Review of Earth and Planetary Science, v. 18, p. 173–204.

Von Damm, K.L., Buttermore, L.G., Oosting, S.E., Bray, A.M., Fornari, D.J., Lilley, M.D., and Shanks, W.C., III, 1997, Direct observation of the evolution of a seafloor "black smoker" from vapor to brine: Earth and Planetary Science Letters, v. 149, p. 101–111.

Wells, M.L., Vallis, G.K., and Silver, E.A., 1999, Tectonic processes in Papua New Guinea and past productivity in the eastern equatorial Pacific Ocean: Nature, v. 398, p. 601–604.

Young, C., and Lupton, J.E., 1983, An ultratight fluid sampling system using cold-welded copper tubing: EOS, v. 64, p. 735.